



Visible-light driven oxidative coupling of amines to imines with high selectivity in air over core-shell structured CdS@C₃N₄



Yong Xu^a, Yong Chen^a, Wen-Fu Fu^{a,b,*}

^a Key Laboratory of Photochemical Conversion and Optoelectronic Materials, CAS-HKU Joint Laboratory on New Materials, Technical Institute of Physics and Chemistry, Chinese Academy of Sciences, University of Chinese Academy of Sciences, Beijing 100049, PR China

^b College of Chemistry and Chemical Engineering, Yunnan Normal University, Kunming 650092, PR China

ARTICLE INFO

Keywords:

CdS@C₃N₄ photocatalyst
Core-shell structure
Photocatalysis
Superoxide radical
Oxidative coupling of amines

ABSTRACT

A core-shell structured CdS@C₃N₄ photocatalyst with a 4 nm thick shell was prepared using self-assembly, and its structure, composition and morphology were characterized in detail. The hybrid visible-light catalyst exhibited a high photocatalytic performance for oxidative coupling of amines under atmospheric conditions, and robust product selectivity up to > 99% for photodriven oxidation of various amines to corresponding imines was achieved. It was confirmed using Hammett-type plots and radical trapping experiments that steric effects and the formation of 'O₂' are critical for photocatalytic conversion of the investigated substrates, and the related catalytic mechanism is presented.

1. Introduction

Solar energy is receiving significant attention as a green, abundant and sustainable energy resource. Consequently, the utilization of sunlight as a driving force for chemical conversion has shown great promise in chemical synthesis. For efficient use of natural light, a photosensitizer is essential to facilitate exciton transfer in the photoreaction. To date, various homogeneous catalytic systems have been reported, such as organometallic complexes and small molecule dyes, because of their long excited-state lifetimes and rich redox potential in the excited state. However, homogeneous photocatalysts suffer from inherent limitations, for instance, low stability during long-term operations, the inclusion of noble metals with restricted availability, and elimination of the catalyst during isolation of the product [1]. In 1972 Fujishima and Honda made a significant breakthrough in the area of photocatalysis, which provides an alternative to traditional chemical synthesis. Heterogeneous photocatalysis can function under mild conditions and the catalysts can be easily recovered and recycled, meeting current energy and environmental requirements [2]. A significant amount of research has been devoted to the use of heterogeneous catalysts for the aerobic oxidation of alcohols, aldehydes and sulfides [3–8].

Imines are significant intermediates in many industrial processes, used to synthesize dyes, pharmaceuticals, fine chemicals and biologically active nitrogen-containing compounds. Traditionally, imines are produced by dehydration condensation of an amine with a compound

containing carboxide [9]. However, the process involves expensive dehydrating agents and the active nature of carbonyl compounds can make the condensation difficult to control. A more dramatic route to imines is the direct oxidation of amines. But the oxidation reagents, such as 2-iodoxybenzoic acid or N-tert-butylphenylsulfinimidoyl chloride, often produce byproducts that are harmful to the environment [9]. By comparison, using molecular oxygen as the oxidant for direct transformation of amines to the corresponding imines can result in an economical and environmentally friendly process. Zhao and coworkers reported that photocatalytic oxidation of aromatic amines to imines, using TiO₂ as a photocatalyst, could be achieved under ultraviolet (UV) irradiation [10]. Tanaka et al. found that amines could be photocatalytically oxidized to imines over Nb₂O₅, which had a wide band gap of 3.2 eV, under visible light irradiation [11]. This is believed that the generated surface complex between Nb₂O₅ and adsorbed amine was the reason for the observed red-shift of light absorption. The formed surface complex could transfer electrons from the amide nitrogen to the conduction band of Nb₂O₅ under visible light. This phenomenon was also discovered in TiO₂ and the mechanism is known as ligand-to-metal charge transfer (LMCT) [11–13]. Dye-sensitized TiO₂ combined with (2,2,6,6-tetramethylpiperidin-1-yl)oxyl (TEMPO) exhibited high activity for selective oxidation of amines to imines under visible light [14]. Au/TiO₂ exhibited high visible-light activity for aerobic oxidation of amines by transferring electrons from the Au nanoparticle to the TiO₂ with the help of a localized surface plasmon resonance (LSPR) effect

* Corresponding author at: Key Laboratory of Photochemical Conversion and Optoelectronic Materials, CAS-HKU Joint Laboratory on New Materials, Technical Institute of Physics and Chemistry, Chinese Academy of Sciences, University of Chinese Academy of Sciences, Beijing 100049, PR China.

E-mail address: fuwf@mail.ipp.ac.cn (W.-F. Fu).

[9]. Wang and coworkers prepared gold nanoclusters, which exhibited high photocatalytic activity for amine oxidation [15]. The catalytically active sites were regarded as the gold atoms exposed upon detaching the PPh_3 ligands. In addition, the high catalytic capacity was derived from the photoexcitation of electrons and holes of the gold nanocluster rather than the LSPR effect. Blechert developed a metal-free protocol for the oxidation of amines by carbon nitride with visible light, however it requires high dioxygen pressure (0.5 MPa) [1]. Jain combined the low cost iron complex with C_3N_4 to give a high yield of imines [16]. Wang and coworkers synthesized biomolecule-derived binary carbon nitride using nucleobases and urea, and the two-dimensional structure allowed for band gap engineering applications [17]. The layered carbonitrides enable the production of an energized charge carrier to facilitate an organic reaction upon light excitation. Metal clusters in metal-organic frameworks (MOFs) can be deemed inorganic semiconductor quantum entities, with the organic linkers acting as antenna, activating the quantum dots by means of linker-to-metal cluster charge transfer (LCCT) under light illumination [18]. Li found $\text{NH}_2\text{-MIL-125(Ti)}$ could generate Ti^{3+} and O_2^- through the reaction between Ti^{3+} and O_2 under irradiation, which could be used for oxidation of amines [19]. The exposed facet of the semiconductor also has a significant influence on amine oxidation, such as was reported for BiVO_4 [20]. Other photocatalysts such as BiOX [21,22], ZnIn_2S_4 [23], WS_2 [24] and CdS [25] have also facilitated the oxidation of amines.

An important challenge for catalyst researchers is the development of a novel, robust and low-cost photocatalyst. Considering the suitable band gap structure and high capacity for visible light absorption, CdS and C_3N_4 were used to design a hybrid photocatalyst [26–28]. The phase junction of two semiconductors can serve as a high-efficiency electron and hole separator. One-dimensional CdS nanowires (CdS NWs) have a number of advantages over other CdS -based materials. These result from their unique structure and large surface area arising from a high ratio of length to diameter, which can enhance light absorption and shorten the transport pathway of photogenerated charge carriers. However, photocorrosion remains a serious problem for CdS NWs, impeding their widespread application. In recent years, metal-free C_3N_4 has received significant interest in photocatalysis due to its excellent chemical stability, visible light response activities and suitable band energy position. Comparing the band edges of CdS and C_3N_4 , the energy levels of CdS and C_3N_4 are well-matched which accelerates electron and hole transfer. Therefore, we can take advantage of both by fabricating a $\text{CdS}/\text{C}_3\text{N}_4$ heterojunction to suppress the photocorrosion of CdS and facilitate charge transfer of C_3N_4 .

2. Experimental

2.1. Material preparation

2.1.1. Preparation of CdS nanowires

All of the reagents were analytical grade and used without further purification. CdS nanowires were prepared according to a previous report with some modification [29]. In a typical process, 0.96 mmol of $\text{Cd(OAc)}_2\text{·}2\text{H}_2\text{O}$ and 3.84 mmol of L-cysteine ($\text{C}_3\text{H}_7\text{NO}_2\text{S}$) were added to a 100 mL Teflon-lined autoclave, followed by 5 mL water by injection. After ultrasonic treatment, a white emulsion was formed, and 43 mL of ethylenediamine was added to the autoclave with stirring to achieve complete dissolution. The autoclave was then sealed and maintained at 180 °C for 24 h. After cooling to room temperature, the yellow product was collected by centrifugation and washed thoroughly with water and ethanol several times. The product was dried in a vacuum oven at 60 °C overnight.

2.1.2. Preparation of C_3N_4

4.0 g of dicyandiamide and 200 mg of barbituric acid were added to 20 mL water, and the mixture was heated at 90 °C with stirring until all water had evaporated. The white solid obtained was calcined at 550 °C

for 4 h in a muffle furnace. The green product was ground into a powder for further use.

2.1.3. Preparation of core-shell structured $\text{CdS@C}_3\text{N}_4$

The as-prepared C_3N_4 was dispersed in 150 mL of ethanol and sonicated for 2 days. The upper suspension was removed and centrifuged to isolate the small C_3N_4 nanosheets. 100 mg of CdS nanowires was added to a 100 mL bottle with 30 mL of ethanol and sonicated, the suspension was then mixed with 15 mg of treated C_3N_4 in 20 mL of ethanol. The mixture was magnetically stirred for 10 h and the final product was obtained by centrifugation and dried under vacuum. This product was denoted $\text{CdS@C}_3\text{N}_4$ (15%). Other photocatalysts were prepared in the same way with different amounts of C_3N_4 .

2.2. Materials characterization

The as-prepared materials were characterized using X-ray powder diffraction (XRD) on a Bruker AXS D8 X-ray diffractometer with $\text{Cu K}\alpha$ ($\lambda = 1.54056 \text{ \AA}$) to identify their crystalline structure and lattice phases. Scanning electron microscopy (SEM) images were conducted on a Hitachi S-4800 field emission scanning electron microscope. The morphologies and lattice fringes of the samples were analyzed on a transmission electron microscope (TEM; JEM 2100 F) with an accelerating voltage of 200 kV. The elemental compositions and distributions of the prepared materials were measured by electron energy loss spectroscopy (EELS). Fourier transform infrared (FTIR) spectroscopy data were collected using the standard KBr disk method at ambient temperature on a Bruker ALPHA FTIR spectrometer over the range of 4000 to 400 cm^{-1} . Ultraviolet-visible diffuse reflectance spectra (DRS) were measured on a spectrophotometer (Hitachi UV-3010) using BaSO_4 as a reference. Photoluminescence spectra (PL) were recorded at room temperature under excitation at 325 nm (Hitachi F-4500). X-ray photoelectron spectroscopy (XPS) was carried out on a PHI 5300 ESCA using an $\text{Al K}\alpha$ X-ray source with a power of 250 W. The charge effect was calibrated using the binding energy of C1 s. The chemical structure and relative quantities of the products were determined using ^1H nuclear magnetic resonance (NMR) spectroscopy (Bruker Avance 400 spectrometer). Electron spin resonance (ESR) signals were recorded at room temperature using a Bruker ESR E500 spectrometer.

2.3. Photocatalytic oxidation of amines

5 mg of photocatalyst was placed in a 15 mL glass tube followed by 4 mL of organic solvent containing 0.3 mmol of amine. The mixture was stirred for 15 min before photoexcitation. White light-emitting diodes (LEDs) ($30 \times 3 \text{ W}$, $\lambda \geq 420 \text{ nm}$) were used as the irradiation light source and the LEDs were placed 3 cm away from the mixture, which was kept stirring continuously at room temperature. After excitation, the mixture was centrifuged and washed 3 times with solvent. The supernatant and washings were collected together and the isolated products were analyzed by ^1H NMR.

3. Results and discussion

3.1. $\text{CdS@C}_3\text{N}_4$ photocatalyst characterization

The crystalline structure and composition of the prepared materials were characterized using XRD, as shown in Fig. 1. Two distinct diffraction peaks of the pure C_3N_4 sample are located at 13.1° and 27.4° ($d = 0.33 \text{ nm}$), which index with the (100) and (002) planes of the graphitic phase respectively. The weak (100) peak can be attributed to the in-plane order of tri-s-triazine units corresponding to the interplanar separation, while the strong (002) peak represents interlamination stacking of conjugated aromatic components [8]. After ultrasonic exfoliation, the intensity of the (100) and (002) peaks reduced significantly, in particular the peak at 27.4°, indicating that interlayer

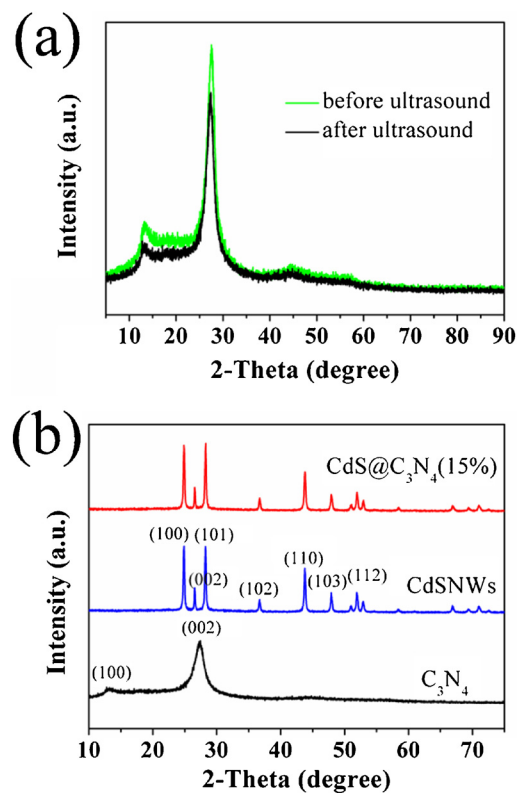


Fig. 1. (a) The comparison of XRD patterns for prepared C_3N_4 and ultrasound-treated C_3N_4 ; (b) XRD patterns of $\text{CdS@C}_3\text{N}_4$ (15%), CdSNWs and C_3N_4 .

structure was disrupted. Pure CdS nanowires exhibit distinguishable diffraction peaks, and are consistent with the hexagonal structure of CdS (JCPDS No. 77-2306, space group: $P63mc$ (186)). The intensity of the (002) peak is clearly low compared with the (100) and (101) peaks, suggesting that CdS NWs preferentially grow along the direction of the c -axis. In Fig. 1(b), the two peaks of C_3N_4 are almost indiscernible in the XRD pattern of $\text{CdS@C}_3\text{N}_4$ due to their low intensity, and the diffraction angle of the (002) facet in C_3N_4 shifts to 28.1° from 27.4° , which is attributed to strong interaction between CdS and the C_3N_4 .

photocatalyst [30].

The detailed morphology and microstructure of the composite photocatalyst was investigated using SEM, TEM and high resolution TEM (HRTEM). The SEM image (Fig. S1) clearly shows that pristine CdS has well-crystallized nanowire morphology with lengths of 2–4 μm . The internal structure can be clearly observed using TEM due to the ability of electrons to penetrate between the shell and the core. It can be seen from Fig. 2 that after formation of the $\text{CdS@C}_3\text{N}_4$ core-shell photocatalyst, the nanostructure of the CdS nanowires is well retained and they have a diameter of 30–50 nm. After a spontaneous adsorption process, the core-shell structured nanowires can be clearly seen, while C_3N_4 is visible as the lamellar structure with intimate contact around the nanowires. HRTEM observation shows that the crystalline core of CdS displays distinct lattice planes of (002) and (100) with d -spacings of 0.33 and 0.36 nm respectively. The thickness of the film-like C_3N_4 layer is ~ 4 nm with a lattice spacing of 0.33 nm corresponding to the (002) facet, indicating that no change occurred in the crystal structure of C_3N_4 after coating on the CdS . During the self-assembly process, C_3N_4 nanosheets adsorb on the surface of CdS NWs, minimizing the total interfacial energy. And the interaction between $-\text{COOH}/-\text{OH}$ and $-\text{NH}_2$ on the surface of CdS NWs and C_3N_4 nanosheets can curl up and wrap around the CdS nanowires, then the adsorbed C_3N_4 assembles into a smooth and compacted shell by a rolling mechanism and a regrowth process. EELS was used to determine the elemental composition and distribution of the core-shell material, and revealed the uniform distribution of C, N, Cd and S over the whole nanowire (Fig. 3), supporting the successful fabrication of the core-shell photocatalyst.

The interaction of the CdS nanowires with C_3N_4 was further examined using FTIR spectroscopy (Fig. 4). The pristine C_3N_4 displays three characteristic absorption peaks in the region of $> 3000 \text{ cm}^{-1}$, 1200 – 1700 cm^{-1} and $< 900 \text{ cm}^{-1}$. The broad C_3N_4 peak between 3000 and 3400 cm^{-1} corresponds to stretching vibrations of terminal $-\text{NH}_2$ or $-\text{NH}-$ groups (3174 cm^{-1}) located at the defect sites of the aromatic ring. The characteristic absorption peaks at 1251 , 1323 , 1422 , 1572 and 1637 cm^{-1} can be ascribed to the typical stretching modes of aromatic carbon nitride heterocycles. And the representative breathing mode of the *s*-triazine units in C_3N_4 can be observed at 810 cm^{-1} . All of the characteristic IR bands are present in the $\text{CdS@C}_3\text{N}_4$ composites, implying that no structural change in C_3N_4 takes place in the course of hybridization. The peaks of the CdS nanowires are not observed, because unlike organic compounds, CdS only shows weak absorption in IR

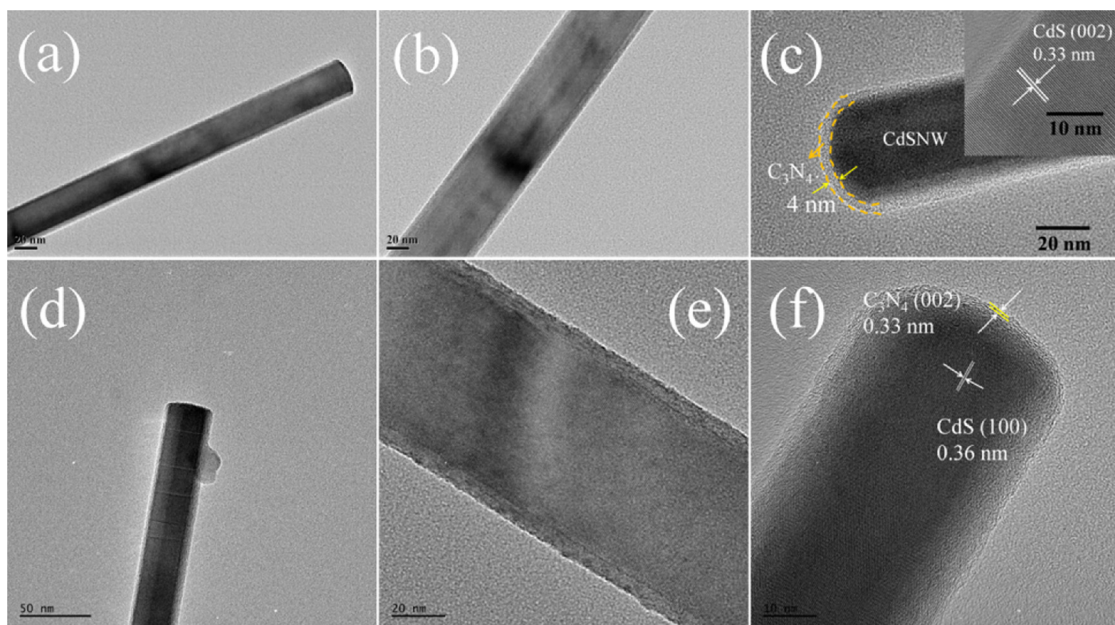


Fig. 2. TEM and HRTEM images of $\text{CdS@C}_3\text{N}_4$ (15%).

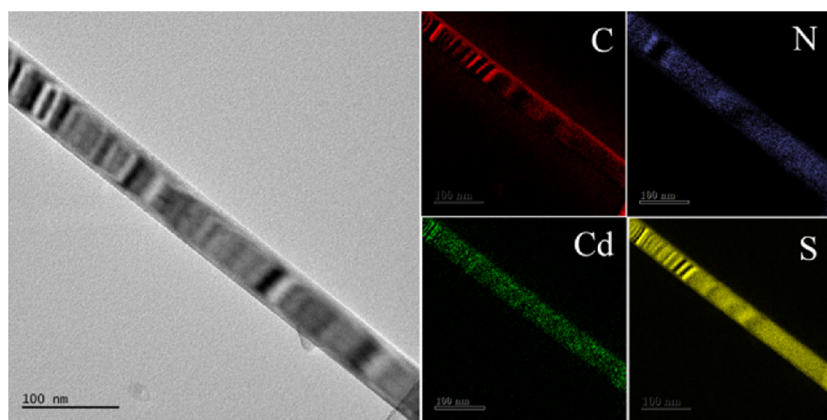


Fig. 3. Elemental composition and distribution of CdS@C₃N₄(15%) measured by EELS.

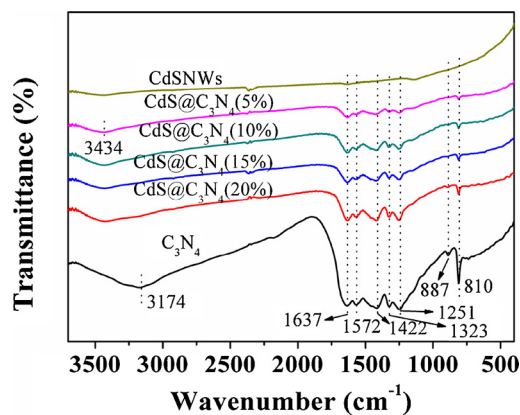


Fig. 4. FTIR spectra of as-synthesized samples.

region. The characteristic peaks of the C₃N₄ phase gradually increase with the increase of the C₃N₄ mass ratio in the composite material. The broad band centered at 3434 cm⁻¹ is attributed to the surface adsorption of water molecules in pure CdS.

Fig. 5 shows Ultraviolet-visible DRS of the as-synthesized samples. As can be seen, the pure C₃N₄ catalyst shows a broad absorption ranging from the ultraviolet to the visible region because of introduced carbon atoms derived from barbituric acid that replaced the nitrogen atoms of the aromatic ring, which modify the electronic structure of C₃N₄ [31]. In comparison with pure CdS, broad background absorption of CdS@C₃N₄ progressively increases in the visible light region. The band gaps of the photocatalysts were determined using the Tauc/Davis-Mott model: $(\alpha h\nu)^{1/n} = A(h\nu - E_g)$, the value of the exponent n is defined as 0.5 for directly allowed transitions. The fitting results illustrate that the band gap of the CdS nanowires is 2.43 eV while that of the modified C₃N₄ is approximately 2.52 eV. On account of the relatively high optical absorption coefficient of C₃N₄, the optical absorptivity of CdS@C₃N₄ shows a slight enhancement with the increase in C₃N₄ content. And the band gaps of the various CdS@C₃N₄ materials are located between those of CdS and C₃N₄. Thus, the formation of a CdS@C₃N₄ heterojunction broadens the range of light absorption, which may efficiently promote conversion of solar energy.

XPS was used to further verify the existence of C₃N₄ in the heterojunction photocatalyst, and obtain insights into the surface chemistry of the materials. The survey spectrum (Fig. 6a) shows that the sample contains C, N, Cd and S elements and a small quantity of O attributed to adsorbed H₂O and CO₂ on the surface of the sample. Fig. 6(b) shows the high resolution XPS spectra of the C 1s, N 1s, Cd 3d and S 2p of CdS@C₃N₄(15%). The C 1s spectrum could be deconvoluted into three

peaks, at 284.8, 286.1 and 288.2 eV. The most intense peak is ascribed to the graphitic sp² carbon-carbon bond, which is usually used as a standard peak. The peak located at 288.2 eV corresponds to a sp²hybridized carbon bonded to a N-containing aromatic structure (N-C = N). The weak peak (286.1 eV) in the middle is attributed to sp³-bonded carbon species from the defects in the C₃N₄ surface [8]. Three peaks centered at 398.9, 400 and 401 eV can be observed from the N 1s spectrum. The peak centered at 398.9 eV is commonly assigned to sp²-bonded nitrogen in the triazine rings (C-N = C)₄. The other two peaks at 400 and 401 eV originate from tertiary nitrogen bonded carbon N-(C)₃and amino groups with a hydrogen atom (C-N-H), respectively [30]. The XPS spectrum of Cd 3d exhibits two distinct single peaks at 404.8 and 411.6 eV, which correspond with the binding energy of Cd 3d_{5/2} and Cd 3d_{3/2}, respectively. Two peaks at 161.2 eV (S 2p_{3/2}) and 162.4 eV (S 2p_{1/2}) are found in the spectra of S 2p, which are assigned to S²⁻ in CdS NWs.

3.2. Photoelectrochemical measurement

Photocurrent response was carried out on a CHI 660 C electrochemical workstation (Chen Hua Instrument) with a conventional tri-electrode system. 0.2 M Na₂SO₄ solution served as the electrolyte, with a platinum foil as the counter electrode and a Ag/AgCl (saturated KCl) reference electrode. The working electrodes were prepared by dropping a slurry of 2 mg photocatalyst and 30 μ L nafion/ethanol (v/v = 1:5) onto conducting indium tin oxide glass (ITO) with an area of 1.0 cm². The film was dried in air at ambient temperature and photoresponse was measured at 0.0 V. As shown in Fig. 7, the transient photocurrent responses of C₃N₄, CdS NWs and CdS@C₃N₄(15%) were measured over several on-off cycles under visible-light illumination. The photocurrent was rapidly generated and increased sharply under photoexcitation, but immediately dropped to zero when the irradiation was stopped. It can be seen from Fig. 7 that the photocurrent intensity of CdS@C₃N₄(15%) is higher than those of pure C₃N₄ and CdS NWs. The generation of a photocurrent is due to the diffusion of photoinduced electrons from the as-prepared photocatalysts to the ITO. Therefore, the enhanced photocurrent indicates that more effective charge transfer and separation is achieved after formation of the core-shell structured composite material. The photocurrent strength is in accordance with the order of photocatalytic activity reported elsewhere [8,32]. To further support the above findings, the photoluminescence spectra were measured at room temperature (Fig. S2). C₃N₄ shows a strong, wide peak with an excitation wavelength of 350 nm, while the emissive intensity of CdS@C₃N₄ is remarkably weakened, indicating that the composite photocatalyst facilitates transfer of charge carriers and reduces the recombination of photogenerated electrons and holes.

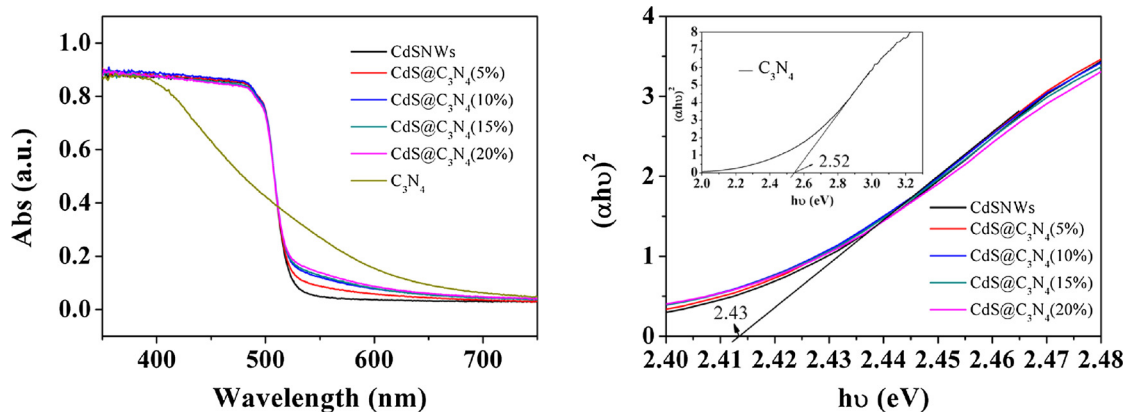


Fig. 5. (a) DRS of CdSNWs, C₃N₄ and CdS@C₃N₄; (b) corresponding plots of $(\alpha h\nu)^2$ versus $(h\nu)$ for the band gap energy.

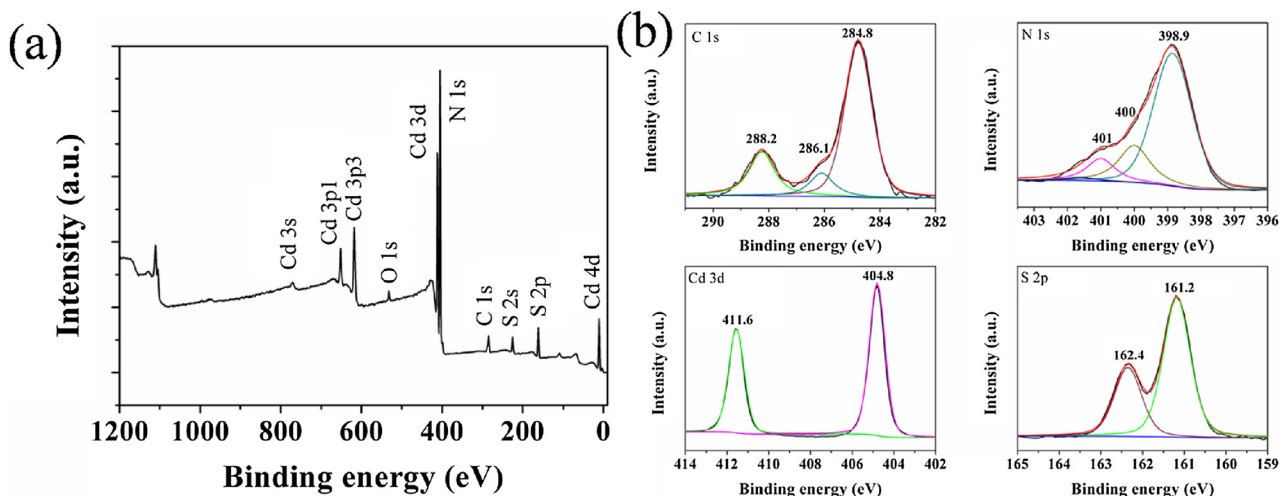


Fig. 6. (a) XPS spectra of CdS@C₃N₄(15%); (b) corresponding high resolution XPS spectra of C 1s, N 1s, Cd 3d and S 2p.

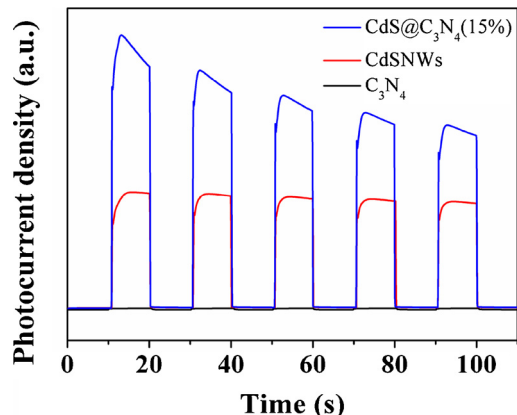


Fig. 7. Transient photocurrent response of C₃N₄, CdSNWs and CdS@C₃N₄(15%).

3.3. Photocatalytic oxidative coupling of amines

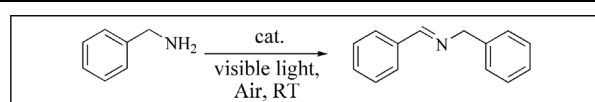
To investigate the photocatalytic performance of the core-shell structured CdS@C₃N₄ for the selective aerobic oxidation of amines to form imines, benzylamine was initially selected as the model substrate, with oxygen in air as the terminal oxidant. As shown in Table 1, benzylamine could be transformed to N-benzylidenebenzylamine with high selectivity (> 99%) under white LED light irradiation at room temperature. Generally, solvents have a significant impact on organic

reactions, the photocatalytic reaction was therefore studied in different solvents (Table 1, entries 1–4), and acetonitrile was found to be the most effective solvent for the oxidative coupling. The photocatalytic activities improved gradually with increasing C₃N₄ content (Table 1, entries 2, 5–6), but when the limiting value was reached, the conversion showed a decline (Table 1, entry 7). This is due to staggered band gap offset occurring between the two semiconductors at the core/shell interface. It was expected that the C₃N₄ coating layer would not improve the light absorption, however, an excess of C₃N₄ in the shell layer obstructs the light absorption and increases the recombination of photo-generated charge carriers in the C₃N₄ shell. The enhanced catalytic performance of CdS@C₃N₄ was attributed to the efficient separation of photo-generated electron-hole pairs. In addition, the catalytic activity of as-prepared CdS@C₃N₄(15%) increased to ~20 times that of native C₃N₄ (Conv. 4.85%), and is 1.7 times that of pure CdS (Conv. 54.35%). A blank experiment was carried out in the absence of light (Table 1, entry 11) and no detectable product was obtained, confirming that the coupling reaction is actually driven by a photocatalytic process. Without addition of photocatalyst or in an environment of 1 atm Ar, very little conversion of the starting substrate was observed, suggesting that the coupling reaction is indeed promoted by oxygen and is associated with the photocatalyst.

As CdS@C₃N₄ is a heterogeneous photocatalyst, it can be easily separated from the reaction solution by filtration or centrifugation. Recycling experiments were carried out to test the photochemical stability of the composite photocatalyst, which is a significant consideration for practical application. The photocatalyst was recycled by centrifugation followed by repeated washing with deionized water and

Table 1

Photocatalytic oxidation of benzylamine with air at room temperature. Reaction conditions: 0.3 mmolbenzylamine, 5 mg photocatalyst, 4 mL solvent, irradiation 4 h.
^aWithout catalyst; ^bIn the dark; ^cAtmosphere of Ar; ^dIrradiation 4.3 h.



entry	catalyst	solvent	conv. (%)	sel. (%)
1	CdS@C ₃ N ₄ (15%)	CH ₃ OH	89.69	> 99
2	CdS@C ₃ N ₄ (15%)	CH ₃ CN	93.46	> 99
3	CdS@C ₃ N ₄ (15%)	EtOAc	64.94	> 99
4	CdS@C ₃ N ₄ (15%)	CH ₂ Cl ₂	78.74	> 99
5	CdS@C ₃ N ₄ (5%)	CH ₃ CN	67.57	> 99
6	CdS@C ₃ N ₄ (10%)	CH ₃ CN	78.43	> 99
7	CdS@C ₃ N ₄ (20%)	CH ₃ CN	78.13	> 99
8	CdS	CH ₃ CN	54.35	> 99
9	C ₃ N ₄	CH ₃ CN	4.85	> 99
10 ^a	—	CH ₃ CN	0	—
11 ^b	CdS@C ₃ N ₄ (15%)	CH ₃ CN	0	—
12 ^c	CdS@C ₃ N ₄ (15%)	CH ₃ CN	0	—
13 ^d	CdS@C ₃ N ₄ (15%)	CH ₃ CN	100	> 99

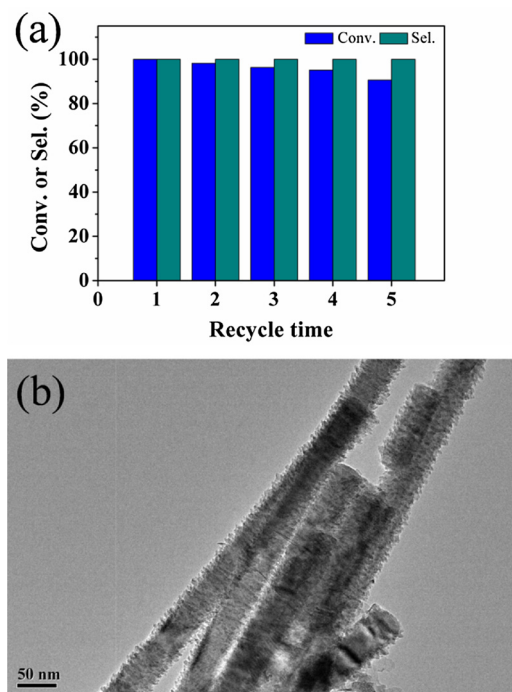


Fig. 8. (a) Cycling tests of benzylamine oxidation catalyzed by CdS@C₃N₄(15%); (b) TEM image after four successive cycles.

ethanol, it was then dried at 60 °C in a vacuum oven. After four continuous cycles (Fig. 8a), only a < 10% decrease in conversion was observed, while the catalytic selectivity remained greater than 99%. The morphology of the photocatalyst after 4 cycles is shown in Fig. 8b. Burrs appeared on the surface of the CdS@C₃N₄, indicating the partial loss of C₃N₄ from the composite photocatalyst.

The catalytic activity of CdS@C₃N₄ was further investigated with various amine derivatives under optimum reaction conditions and the results are listed in Table 2. Benzylamines with either electron-donating or -withdrawing substituent groups (Table 2, entries 2–8) gave good conversion to the corresponding imines with excellent selectivity ($\geq 99\%$). Compared with previous reports [15,19,23–25], steric effects have a larger influence on conversion than electronic effects for this system. Compared with benzylamine, the aromatic amines with substituents on the phenyl ring showed decreased conversion due to steric

hindrance (Table 2, entries 2–4). When there is a methyl at the α -C of benzylamine (Table 2, entry 9), the conversion rate was further reduced. A secondary amine, could be oxidized to the corresponding imine (Table 2, entry 10), but only 6.1% conversion was obtained. Although steric effects have a significant impact on conversion, excellent selectivity is achieved for all amines. Moreover, the system could also efficiently convert a heteroatom amine to the corresponding imine (Table 2, entry 11). We used the Hammett equation, which describes the linear free-energy relationship between reaction rate (and equilibrium constant) and the type of reactant substituent, to study the effect of substituent on conversion. A series of kinetics experiments were carried out using benzylamine derivatives with various groups such as $-\text{CH}_3$, $-\text{OCH}_3$, $-\text{F}$, $-\text{Cl}$ and $-\text{CF}_3$ as reactants (Fig. S3a). The slopes of the linear plots give ρ values that do not have a linear or bilinear relationship (Fig. S3b), indicating that a steric rather than an electronic effect plays a major role.

3.4. Mechanistic investigation

In general, it is believed that the aerobic oxidation of amines to the corresponding imines proceeds via a pathway of oxygenation. To get an insight into the photocatalytic oxidation mechanism, an ESR spin-trapping experiment with 5,5'-dimethyl-1-pyrroline N-oxide (DMPO) was conducted to study the reactive oxygen species produced during light illumination. The detected signal reveals four groups of characteristic peaks (Fig. 9, red curve), indicating that the DMPO- O_2 adduct is formed during the photochemical reaction. In addition, it is thermodynamically stable for the photogenerated electrons to transfer to the adsorbed O_2 to form superoxide radicals (O_2^-). However, when adding benzylamine to the catalytic system, the peak strength was distinctly weakened (Fig. 9, blue curve), which suggests that the superoxide radical is crucial in the oxygenation of amines. To acquire more information on photogenerated radical species in photocatalytic redox reactions, controlled experiments were carried out. The effect of different radical quenchers on photocatalytic benzylamine oxidation is shown in Fig. 10. When *p*-benzoquinone was injected into the photoreaction system, the conversion dropped to 15.9% compared with a conversion of 100% in the absence of quenching agent. This result reveals that the superoxide radical formed is the major active oxidation species involved in the selective oxidation of amine to imine. Clear decreases in the photo-oxidation activities were observed when $\text{K}_2\text{S}_2\text{O}_8$ (quenching electrons) and ammonium oxalate (quenching holes) were employed as quenchers in the photocatalytic reaction. It can therefore be concluded that both photogenerated electrons and holes may be initial drivers for photocatalytic oxidation. These active species

Table 2

Photocatalytic oxidation of various amines over CdS@C₃N₄(15%). Reaction conditions: 0.3 mmol amine, 5 mg CdS@C₃N₄(15%), 4 mL acetonitrile, visible light irradiation, room temperature.

entry	substrate	product	time (h)	conv. (%)	sel. (%)
				conv. (%)	sel. (%)
1	<chem>Cc1ccccc1N</chem>	<chem>Cc1ccccc1C=NNCc2ccccc2</chem>	4.3	100	>99
2	<chem>Cc1ccccc1N</chem>	<chem>Cc1ccccc1C=NNCc2ccccc2</chem>	5.3	93.5	>99
3	<chem>Cc1ccccc1N</chem>	<chem>Cc1ccccc1C=NNCc2ccccc2</chem>	8.1	100	>99
4	<chem>Cc1ccccc1N</chem>	<chem>Cc1ccccc1C=NNCc2ccccc2</chem>	9	68.5	>99
5	<chem>FC(F)(F)Cc1ccccc1N</chem>	<chem>FC(F)(F)Cc1ccccc1C=NNCc2ccccc2</chem>	6	61.7	>99
6	<chem>OCOCc1ccccc1N</chem>	<chem>OCOCc1ccccc1C=NNCc2ccccc2</chem>	5.3	56.0	99
7	<chem>FC(F)Cc1ccccc1N</chem>	<chem>FC(F)Cc1ccccc1C=NNCc2ccccc2</chem>	6	93.0	>99
8	<chem>ClCc1ccccc1N</chem>	<chem>ClCc1ccccc1C=NNCc2ccccc2</chem>	5.1	100	>99
9	<chem>Cc1ccccc1C(N)(C)C</chem>	<chem>Cc1ccccc1C(N)(C)=NNCc2ccccc2</chem>	9	31.1	>99
10	<chem>Cc1ccccc1NCCc2ccccc2</chem>	<chem>Cc1ccccc1C=NNCc2ccccc2</chem>	9	6.1	>99
11	<chem>O=C1OC(F)(F)C(F)(F)C1N</chem>	<chem>O=C1OC(F)(F)C(F)(F)C1C=NNCc2ccccc2</chem>	6.5	79.1	>99

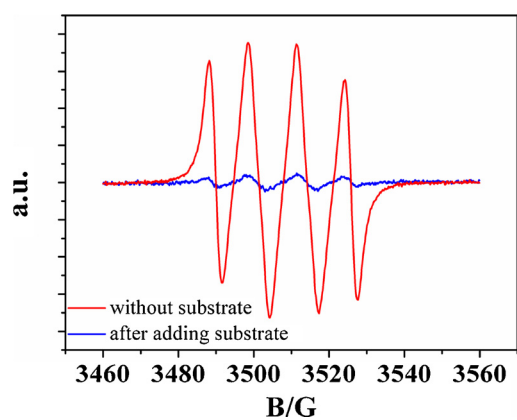


Fig. 9. ESR spectra for a system containing DMPO and CdS@C₃N₄(15%) in acetonitrile upon irradiation with visible light in air.

trapping experiments demonstrated that molecular oxygen combined with photogenerated electrons from the conduction band to yield superoxide radicals, thus improving the separation efficiency of electrons and holes.

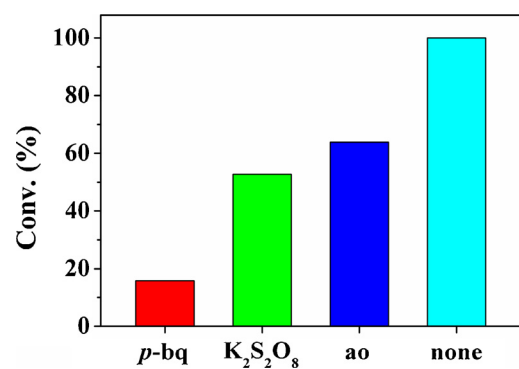


Fig. 10. Quenching experiment using different radical scavengers for photocatalytic benzylamine oxidation over CdS@C₃N₄(15%).

On the basis of the above results, the mechanism shown in Fig. 11 is proposed for the oxidative coupling of amines catalyzed by CdS@C₃N₄. Under the irradiation of visible light, electrons are excited to the conduction band from the valence band of CdS and C₃N₄, leaving holes in the valence band. The electrons in the conduction band of CdS can be trapped by electrophilic O₂ to produce superoxide radical anions, as

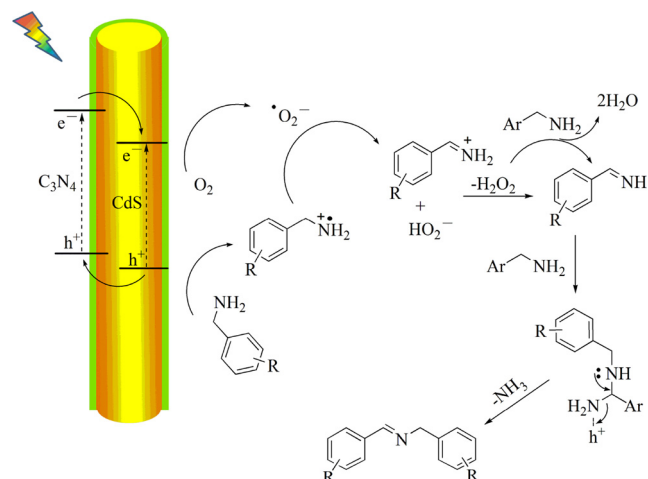


Fig. 11. Proposed mechanism for photo-oxidation of amine catalyzed by CdS@C₃N₄.

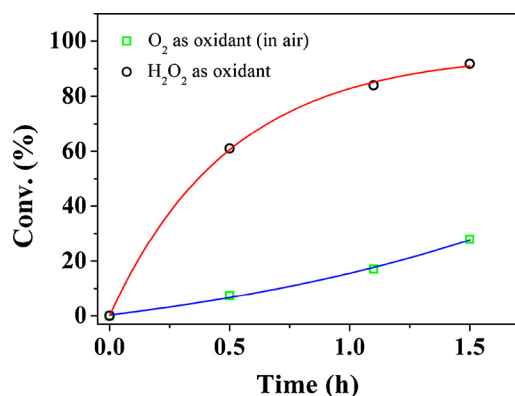


Fig. 12. Time-dependent catalytic performances over CdS@C₃N₄(15%) using O₂ and H₂O₂ as oxidants. Reaction conditions: 0.3 mmol benzylamine, 5 mg CdS@C₃N₄(15%), 4 mL acetonitrile, H₂O₂ (3 equiv.), visible light irradiation, room temperature.

confirmed by ESR. The amine donates an electron to the valence band to yield a benzylamine radical cation [15]. Subsequently, the superoxide radical anion abstracts a proton from the amine radical cation as well as an adjacent hydrogen atom forming Ph-CH = NH and H₂O₂. The H₂O₂ was detected by color change by adding KMnO₄, as illustrated in Fig. S4. Notably, the Ph-CH = NH species is very reactive during the photocatalytic process. The intermediate is prone to nucleophilic attack by benzylamine to produce an aminal (Ph-CH₂-NH-CH(NH₂)-Ph). Elimination of the terminal amino group and adjacent hydrogen atom then results in the formation of a coupled product. When H₂O₂ was used as the oxidant instead of O₂, the catalytic reaction proceeded more quickly (Fig. 12), which suggests that peroxide species may be the reactive intermediate.

4. Conclusion

In summary, we successfully fabricated a core-shell structured CdS@C₃N₄ hybrid visible light catalyst with a 4 nm shell layer and applied it as a photocatalyst. The photocatalyst achieved oxidative coupling of various amines with high conversion efficiency of the substrate and product selectivity for imines in air. The enhanced photocatalytic activity arises from the well-matched band gap structure and closely contacted heterojunction interface of the materials, thereby

improving separation efficiency of photogenerated electrons and holes. Superoxide radicals detected using ESR and a quenching experiment showed that 'O₂ played a crucial part in amine oxygenation, and an investigation of the steric and electronic effects on conversion efficiency revealed that the former is more important in the studied system.

Acknowledgements

This work was financially supported by the National Key Basic Research Program of China (973 Program 2013CB834804) and the Ministry of Science and Technology (2012DFH40090) and the Strategic Priority Research Program of the Chinese Academy of Sciences (XDB17030200). We thank the Natural Science Foundation of China (21267025, 21367026, 21471155) for financial support.

Appendix A. Supplementary data

Supplementary material related to this article can be found, in the online version, at doi: <https://doi.org/10.1016/j.apcatt.2018.03.098>.

References

- [1] F. Su, S.C. Mathew, L. Möhlmann, M. Antonietti, X. Wang, S. Blechert, *Angew. Chem. Int. Ed.* 50 (2011) 657–660.
- [2] A. Fujishima, K. Honda, *Nature* 238 (1972) 37–38.
- [3] Z. Chai, T.-T. Zeng, Q. Li, L.-Q. Lu, W.-J. Xiao, D. Xu, *J. Am. Chem. Soc.* 138 (2016) 10128–10131.
- [4] Y.-Z. Chen, Z.-U. Wang, H. Wang, J. Lu, S.-H. Yu, H.-L. Jiang, *J. Am. Chem. Soc.* 139 (2017) 2035–2044.
- [5] L. Yu, Y. Lin, D. Li, *Appl. Catal. B: Environ.* 216 (2017) 88–94.
- [6] S. Meng, X. Ye, X. Ning, M. Xie, X. Fu, S. Chen, *Appl. Catal. B: Environ.* 182 (2016) 356–368.
- [7] X. Lang, W.R. Leow, J. Zhao, X. Chen, *Chem. Sci.* 6 (2015) 1075–1082.
- [8] Y. Xu, Z.-C. Fu, S. Cao, Y. Chen, W.-F. Fu, *Catal. Sci. Technol.* 7 (2017) 587–595.
- [9] S. Naya, K. Kimura, H. Tada, *ACS Catal.* 3 (2013) 10–13.
- [10] X. Lang, H. Ji, C. Chen, W. Ma, J. Zhao, *Angew. Chem. Int. Ed.* 50 (2011) 3934–3937.
- [11] S. Furukawa, Y. Ohno, T. Shishido, K. Teramura, T. Tanaka, *J. Phys. Chem. C* 117 (2013) 442–450.
- [12] N. Li, X. Lang, W. Ma, H. Ji, C. Chen, J. Zhao, *Chem. Commun.* 49 (2013) 5034–5036.
- [13] X. Lang, W. Ma, Y. Zhao, C. Chen, H. Ji, J. Zhao, *Chem. Eur. J.* 18 (2012) 2624–2631.
- [14] Z. Wang, X. Lang, *Appl. Catal. B: Environ.* 224 (2018) 404–409.
- [15] H. Chen, C. Liu, M. Wang, C. Zhang, N. Luo, Y. Wang, H. Abroshan, G. Li, F. Wang, *ACS Catal.* 7 (2017) 3632–3638.
- [16] A. Kumar, P. Kumar, C. Joshi, S. Ponnada, A.K. Pathak, A. Ali, B. Sreedhar, S.L. Jain, *Green Chem.* 18 (2016) 2514–2521.
- [17] C. Yang, B. Wang, L. Zhang, L. Yin, X. Wang, *Angew. Chem. Int. Ed.* 56 (2017) 6627–6631.
- [18] T. Tachikawa, J.R. Choi, M. Fujitsuka, T. Majima, *J. Phys. Chem. C* 112 (2008) 14090–14101.
- [19] D. Sun, L. Ye, Z. Li, *Appl. Catal. B: Environ.* 164 (2015) 428–432.
- [20] B. Yuan, R. Chong, B. Zhang, J. Li, Y. Liu, C. Li, *Chem. Commun.* 50 (2014) 15593–15596.
- [21] Y. Wu, B. Yuan, M. Li, W.-H. Zhang, Y. Liu, C. Li, *Chem. Sci.* 6 (2015) 1873–1878.
- [22] A. Han, H. Zhang, G. Chuah, S. Jaenicke, *Appl. Catal. B: Environ.* 219 (2017) 269–275.
- [23] L. Ye, Z. Li, *ChemCatChem* 6 (2014) 2540–2543.
- [24] F. Raza, J.H. Park, H.-R. Lee, H.-I. Kim, S.-J. Jeon, J.-H. Kim, *ACS Catal.* 6 (2016) 2754–2759.
- [25] W. Zhao, C. Liu, L. Cao, X. Yin, H. Xu, B. Zhang, *RSC Adv.* 3 (2013) 22944–22948.
- [26] R.C. Pawar, V. Khare, C.S. Lee, *Dalton Trans.* 43 (2014) 12514–12527.
- [27] X. Ye, X. Dai, S. Meng, X. Fu, S. Chen, *Chin. J. Chem.* 35 (2017) 217–225.
- [28] J. Zhang, Y. Wang, J. Jin, J. Zhang, Z. Lin, F. Huang, J. Yu, *ACS Appl. Mater. Interfaces* 5 (2013) 10317–10324.
- [29] J. Yu, Y. Yu, P. Zhou, W. Xiao, B. Cheng, *Appl. Catal. B: Environ.* 156–157 (2014) 184–191.
- [30] X. Ye, X. Dai, S. Meng, X. Fu, S. Chen, *Chin. J. Chem.* 35 (2017) 217–225.
- [31] J. Zhang, Y. Wang, J. Jin, J. Zhang, Z. Lin, F. Huang, J. Yu, *ACS Appl. Mater. Interfaces* 5 (2013) 10317–10324.
- [32] M. Lu, Z. Pei, S. Weng, W. Feng, Z. Fang, Z. Zheng, M. Huang, P. Liu, *Phys. Chem. Chem. Phys.* 16 (2014) 21280–21288.